Communications on Applied Nonlinear Analysis
ISSN: 1074-133X
Vol 32 No. 1 (2025)

Numerical Study of the 3D MHD Radiative Flow of Williamson Nanofluid with Variable Characteristics Over a Double Stretching Sheet

Boreddy Mahendar Reddy[1], Mattipelli Ramachandru[2*], Kambampati Satyanarayana[3], Naikoti Kishan[4]

[1, 3, 4] Department of mathematics, UCS, Osmania University, Hyderabad, Telangana, India-500007
[2*] Department of Humanities and science, UCET, Mahatma Gandhi University, Telangana, India-508254,
[1]reddym195@gmail.com, [2*]ramanmaths7@gmail.com, [3]satyamaths123@gmail.com, [4]kishan.naikoti@gmail.com
[*]Corresponding Author: Email: ramanmaths7@gmail.com

Article History:

Received: *17-07-2024*

Revised: *30-08-2024*

Accepted: *12-09-2024*

Abstract:
The current study investigates the influence of variable thermal conductivity and mass conductivity on 3D MHD. The significance of this study lies in mass diffusion on a three-dimensional Williamson nanofluid fluid flow over a double stretched sheet. When thermal radiation and Hall current is present, the heat transfer process is explored to see how chemical reactions affect heat and mass transmission. Additional phenomena, such as momentum slip and convective boundary conditions, contribute to the model's uniqueness. The problem formulation becomes ordinary differential equations with application of the Von Karman similarity variable. Use of the bvp4c function in yields a numerical solution for the system of differential equations. Using MATLAB's bvp4c function, a numerical solution to the differential equation system is obtained. A graphic is used to discuss the overall result of several metrics compared to the involved profiles. It is believed that as temperature-dependent thermal conductivity and viscosity increase, so does the temperature field. When the Williamson fluid and magnetic parameters rise, the velocity field decays in the x- and y-axis directions. To support the identified issue, a comparison between the current inquiry and a previously published work is also included.

Keywords: Williamson nanofluid, thermal radiation, MHD, Chemical reaction, Variable Viscosity.

1. Introduction

The exploration of non-Newtonian fluid dynamics, especially those exhibiting variable properties, holds paramount importance across a multitude of industrial and engineering domains, including polymer processing, food manufacturing, and biomedical engineering. A critical component of these fluids is their reaction to thermal influences, which can profoundly affect their flow behavior and heat transfer properties. The studies delve into the traits of 3D fluid flows with Maxwell fluids that have changing properties like viscosity and thermal conductivity. These studies investigate the effects of temperature, shear rate, and magnetic fields on the flow behavior of such fluids. Imtiaz [1] investigated the effects of factors such as the Maxwell fluid parameter, thermal radiation parameter, Schmidt number, and Prandtl number on velocity, temperature, and mass transfer rates. Furthermore, the Cattaneo-Christov double diffusion model is used to assess flow over bi-directional stretching surfaces, taking into account concentration-dependent diffusivity, temperature-dependent dynamic

viscosity, and thermal conductivity, as investigated by Upreti et al, [2]. The findings highlight the importance of knowing how these factors influence fluid dynamics and heat transfer processes in complicated flow settings, which may provide useful insights for industrial applications. The viscosity of the fluid is modeled through an Arrhenius-type relationship, while the heat necessary for melting is depicted as a source term within the energy equation by Sinha et al. [3]. A numerical analysis of a steady biomagnetic fluid flow (BFD) driven by a magnetic dipole across a two-dimensional stretching sheet with variable viscosity and thermal conductivity was carried out in the paper by Murtaza et al.[4]. Using the concepts of magnetohydrodynamics (MHD) and ferrohydrodynamics (FHD), the model treated blood as a polarized, electrically conducting fluid. Furthermore, the effect of boundary slip on fluid dynamics in sedimentary formations with low permeability emphasizes the necessity of taking slip conditions into account in complicated porous systems, particularly when working with the heterogeneous structures that Muzemder & Singh [5] analyzed. Moreover, the examination of fluid-structure interactions in three-dimensional domains using Navier's slip interface conditions highlights the significance of taking into account various slipping conditions at fluid-structure interfaces instead of depending exclusively on the conventional no-slip boundary condition studied by Fara et al. [6]. In many industrial applications, it is essential to understand 3D flow with varying viscosity and liquid characteristics, especially Maxwell fluids. Due to their dual viscous and elastic characteristics, Maxwell fluids are useful in the polymeric industries that Sudarmozhi et al. [7] studied. The significance of taking into account variable characteristics in fluid dynamics investigations is demonstrated by Muhammad et al. [8] observation that the impact of concentration- and temperature-dependent diffusivity and viscosity on flow behavior has been investigated. Numerous studies have been conducted on the changing characteristics of liquid in magnetohydrodynamic (MHD) fluid flow in a variety of settings. In their investigation of the effects of changing fluid characteristics on the temperature and velocity fields during peristaltic motion of a third-grade fluid, Choudhari et al. [9] found that these fields were less affected. In an unsteady MHD free stream flow across a stretched sheet, Taneja et al. [10] investigated the effects of varying fluid viscosity and thermal diffusivity on heat and flow behavior, emphasizing the transition points in velocity profiles and the impact of magnetic fields.

The constant three-dimensional flow and heat transmission of three different kinds of water-based nanoparticles copper (Cu), aluminum oxide (Al2O3), and titanium dioxide (TiO2) due to stretching sheets in the presence of heat sources and magnetic fields were studied by Tarakaramu et al. [11]. The study by C et al. [12] explores the analysis of magneto hydrodynamic boundary layer flow with heat and mass transfer of Williamson nanofluid over a stretched sheet featuring variable thickness and variable thermal conductivity. Nanofluids with mass fractions of 0.1%, 0.3%, and 0.5% were produced by Sun et al.[13] researchers using nanoparticles (Cu, Fe2O3, and Al2O3) with average particle sizes of 50 nm. They employed different concentrations of dispersants, such as sodium dodecyl benzene sulfonate (SDBS), to increase the stability of the nanofluids. Additionally, they looked at the nanofluids' capacity for convective and flow heat transfer in a plate heat exchanger. Sheikholeslami and Rokni [14] investigated the laminar nanofluid heat and mass transfer between two contracting and revolving surfaces. The Buongiorno model is employed to model nanofluids. Prasannakumara et al. [15] have studied the similar and different chemical processes that affect the movement of a three-dimensional electrically conducting flux that contains titan dioxide and a

nanofluid based on ethylene glycol as it passes through a tendue containing NP aggregates. Alhazmi & Ahmed [16] used the Cattaneo–Christov double-diffusion theory approach to study the 3-dimensional (3D) induced flow of second-grade viscous nanofluids across a permeable stretched surface. The effects of Maxwell and Smoluchowski temperature variations on the magnetohydrodynamic (MHD) debit of the hybrid nanofluid on a tilted surface have been studied by Rafique et al.[17]. Aziz et al. [18] have qualitatively examined the impact of various parameters on the system's thermal performance. Include the effects of varied thermal conduction and variable viscosity on the heat-transfer characteristics and flux of a Power-Law type nanofluid. The combined effect of Soret and Dufour with temperature-dependent viscosity, as well as radiation, chemical reaction, and porosity, were studied by Mishra et al. [19] on inclined composite stenosis. Rehman et al. [20] investigated the effects of varying viscosity in an infinite disc and Marangoni (MC) convection in the engine oil as a base fluid with viscosity dissipation. The flow system takes into account the effects of the changeable viscosity, the convective boundary conditions, and the viscosity dispersion. Ali et al. [21] investigated the temperature-dependent viscosity's effect on the magnetohydrodynamic boundary layer-Nanofluid flow with double stratification using the Cattaneo-Christov Heat flux Models. In his research, Basha [22] investigated an interface that might be expanded in two ways. One is persuaded to assume that nanoparticles have an undetected mass flux. In addition, the flow model accounts for a source of heat generation or absorption and slip conditions at speed.

The above mentioned literature only focuses on investigations. In this process, the effect of temperature-dependent viscosity on the magnetohydrodynamic boundary layer flow is investigated in order to analyze the heat transfer with double stratification through a stretching-sheet in Williamson nanofluids. Considering the thermal radiation and Hall current and this model is significant because it allows for a more accurate estimation of temperature distribution. It is assumed that the viscosity of the fluid decreases as temperature increases. A Reynolds exponential viscosity model was considered in light of this framework. In order to solve converted assembly equations, the RK-4th order method was applied. MATLAB software was used for programming in this instance. The goal of this study is to thoroughly examine how various types of parameters and thermodynamic conductivities behave through a detailed discussion. Additionally, a numerical evaluation of the current results is shown and reflected in the figures.

The vast range of applications in industrial and technical processes, together with their complicated character, have drawn substantial interest to the examination of magnetohydrodynamic (MHD) fluxes, especially those using non-Newtonian liquids like Williamson nanofluid. When variables such varied viscosity, dynamic liquid properties, and chemical reactivity are taken into account, the study significantly gets more complex. We cover here the 3D MHD flow of chemically reactive Williamson nanofluid with thermal radiation effect, which also show variations in viscosity and liquid properties.

2. Mathematical Formulation

This study examined a steady, viscous, and incompressible flow of nanofluid in three dimensions (3D) under the auspices of the Williamson model on a bidirectional stretching surface subjected to slip conditions in terms of velocity, convection conditions in terms of thermal state, and flux of

nanoparticles conditions in terms of particle concentration. The flow's geometry is restricted to $z = 0$, and it occurs in the domain $z > 0$. Additionally, the Cartesian coordinate system is chosen so that the liquid is occupied at $z \geq 0$ and the feather is associated with the xy- plane (see Fig. 1).

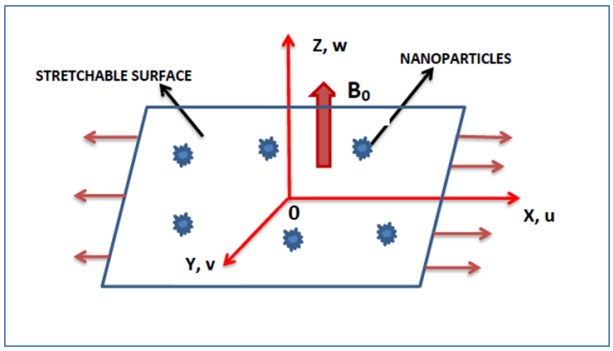

Figure.1 Physical Interpretation of the flow

In the first-order chemically reactive nanofluid, the influence of the thermal radiation and also referred heat generation or absorption. The liquid is electrically conducted, and an applied magnetic strength Bo acts transversely to the flow in the z-a direction. The prevailing equations for an incompressible, non-Newtonian Williamson nanofluid are typical mass conservation, thermal energy, and species nanoparticle equations, using the customary boundary layer approximation:

$$u_x + u_y + u_z = 0 \tag{1}$$

$$uu_x + vu_y + wu_z = \frac{1}{\rho_f}\left(\frac{\partial}{\partial z}\mu(T)\frac{\partial u}{\partial z}\right) - \frac{\sigma B_0^2}{\rho_f}u + \sqrt{2\nu}\Gamma\frac{\partial u}{\partial z}\frac{\partial^2 u}{\partial z^2} \tag{2}$$

$$uv_x + vv_y + wv_z = \frac{1}{\rho_f}\left(\frac{\partial}{\partial z}\mu(T)\frac{\partial v}{\partial z}\right) - \frac{\sigma B_0^2}{\rho_f}v + \sqrt{2\nu}\Gamma\frac{\partial v}{\partial z}\frac{\partial^2 v}{\partial z^2} \tag{3}$$

$$u\frac{\partial T}{\partial x} + v\frac{\partial T}{\partial y} + w\frac{\partial T}{\partial z} = \frac{\partial}{\partial z}\left(\alpha_f(T)\frac{\partial T}{\partial z}\right) + \tau\left(D_B(C)\frac{\partial C}{\partial Z}\frac{\partial T}{\partial z} + \frac{D_T}{T_\infty}\left(\frac{\partial T}{\partial z}\right)^2\right) - \frac{1}{(\rho c)_f}\left(\frac{\partial q_r}{\partial z}\right) + \sigma B_0^2(u^2 + v^2) \tag{4}$$

$$u\frac{\partial C}{\partial x} + v\frac{\partial C}{\partial y} + w\frac{\partial C}{\partial z} = \frac{\partial}{\partial z}\left(D_B(C)\frac{\partial C}{\partial z}\right) + \frac{D_T}{T_\infty}\left(\frac{\partial^2 T}{\partial z^2}\right) - k_c(C - C_\infty) \tag{5}$$

The equations u, v, and w indicate the velocity components in the x, y and z-directions, respectively, describing the fluid's flow in three dimensions. The liquid's temperature (T) can affect its characteristics. The constant density of a liquid ρ_f determines its mass and behavior under different forces. μ_f is the coefficient of viscosity, which describes the fluid's resistance to flow and shear. Finally, μ are inverse temperature functions that impact the fluid's viscosity and other thermodynamic characteristics.

$$\mu = \frac{\mu_f}{1+\chi_f(T-T_\infty)};\ c = \frac{\chi_f}{\mu_f};\ \mu_f = \frac{1}{c(T-T_r)};\ \text{and}\ T_r = T_\infty - \frac{1}{\chi_f} \tag{6}$$

Here c is the constant illustrates fluid type, with $c < 0$ indicating gasses and $c > 0$ representing liquids. T_∞ , μ_f are constants thermal and coefficients of viscosity at a distance far away from the sheet, χ_f feature of hot fluid. While C_P indicates specific heat, Electrical conductivity is represented by S, and specific heat is represented by Cp. Additionally, the temperature is represented by the heat

conductivity K(T) and the species depending on the molecular dispersion of diffusing species $D_B(C)$ are provided to fluctuate as direct functions of the respective types of thermal and species diffusion:

$$\alpha_f = \frac{k_f}{\rho_f c_p};\ \frac{K(T)}{\rho_f c_p} = \frac{k_f}{\rho_f c_p}\left(1 + \varepsilon_1 \frac{(T_\infty - T)}{T_\infty - T_w}\right),\ D_B(T) = D_{Bf}\left(1 + \varepsilon_2 \frac{C_\infty - C}{C_\infty - C_w}\right) \tag{7}$$

The symbols $\varepsilon_1$and ε_2 likely represent variable conductivity and a species parameter, respectively. Consider k_f and D_{Bf}these figures likely represent thermal conductivity k_f and species dispersion D_{Bf} far from the surface. The Thermophorotic force coefficient D_T describes the force on particles in a fluid due to a temperature gradient.ϕ: This parameter is given by $\tau = \frac{(\rho_f c_p)_p}{(\rho c_p)_f}$ is the effective heat capacity of nanoparticles is compared to the fluid heat capacity. When equations (6) and (7) are substituted into equations (2-4) and (5), a new set of equations is formed that includes the expressions described in (6) and (7). These new equations are likely to characterize the system's behavior in more depth or specificity, perhaps accounting for the impact of factors such as conductivity, species characteristics, thermal conductivity, and thermophoresis forces.

$$uu_x + vu_y + wu_z = \frac{1}{\rho_f}\frac{\partial}{\partial z}\left(\frac{\mu_f}{1+\chi_f(T-T_\infty)}\frac{\partial u}{\partial z}\right) - \frac{\sigma B_0^2}{\rho_f}u + \sqrt{2v_f}\Gamma\frac{\partial u}{\partial z}\frac{\partial^2 u}{\partial z^2} \tag{8}$$

$$uv_x + vv_y + wv_z = \frac{1}{\rho_f}\frac{\partial}{\partial z}\left(\frac{\mu_f}{1+\chi_f(T-T_\infty)}\frac{\partial v}{\partial z}\right) - \frac{\sigma B_0^2}{\rho_f}v + \sqrt{2v}_{\mathrm{f}}\Gamma\frac{\partial v}{\partial z}\frac{\partial^2 v}{\partial z^2} \tag{9}$$

$$uT_x + vT_y + wT_z = \frac{\partial}{\partial z}\left(\alpha_f\left(1 + \varepsilon_1\frac{(T_\infty - T)}{T_\infty - T_w}\right)\frac{\partial T}{\partial z}\right) + \tau\left(D_{Bf}\left(1 + \varepsilon_2\left(\frac{C_\infty - C}{C_\infty - C_w}\right)\frac{\partial C}{\partial z}\frac{\partial T}{\partial z}\right) + \frac{D_T}{T_\infty}\left(\frac{\partial T}{\partial z}\right)^2\right) + \frac{16\sigma T_\infty^3}{3k^*\rho_f c_p}\frac{\partial^2 T}{\partial z^2} + \frac{\sigma B_0^2}{\rho_f c_p}(u^2 + v^2) \tag{10}$$

$$uC_x + vC_y + wC_z = \frac{\partial}{\partial z}\left(D_{Bf}\left(1 + \varepsilon_2\frac{C_\infty - C}{C_\infty - C_w}\right)\frac{\partial C}{\partial z}\right) + \frac{D_T}{T_\infty}\frac{\partial^2 T}{\partial z^2} - K_c(C - C_\infty) \tag{11}$$

The linked and utilized boundary conditions are:

$$\left.\begin{gathered} u = u_w = k_1\frac{\partial u}{\partial z} + ax;\ v = v_w = k_2\frac{\partial v}{\partial z} + by;\ w = 0;\ k_f\frac{\partial T}{\partial z} = h_f(T - T_f);\ C = C_w\ at\ z = 0 \\ u = 0;\ v = 0;\ T \to T_\infty;\ C \to C_\infty \text{ as } z \to \infty \end{gathered}\right\} \tag{12}$$

Where h_f is the heat flux coefficient, T_f is the temperature of the hot liquid, a and b are positive constants. In mathematical modeling non-dimensional variables are a common tactic for simplifying equations and exposing underlying relationships across diverse physical scenarios. Scaling variables are commonly used in this process (see details Vaidya et al.[23]).

Similarity transformations

$$\left.\begin{gathered} (u, v, w) = \left(axf'(\eta),\ ayg'(\eta),\ -\sqrt{2v}\left(f(\eta) + g(\eta)\right)\right) \\ (T, C) = (T_\infty + (T_w - T_\infty)\theta(\eta),\ C_\infty + (C_w - C_\infty)\Phi(\eta)) \end{gathered}\right\} \tag{13}$$

Through this similarity transformation equations (8)-(11) transformed as

$$\frac{f'''}{\left(1 - \frac{\theta}{\theta_r}\right)} + \frac{\theta' f''}{\theta_r\left(1 - \frac{\theta}{\theta_r}\right)^2} + Wef''f''' + (f + g)f'' - f'^2 - Mf' = 0 \tag{14}$$

$$\frac{g'''}{\left(1-\frac{\theta}{\theta_r}\right)}+\frac{\theta' g''}{\theta_r\left(1-\frac{\theta}{\theta_r}\right)^2}+Weg''g'''+(f+g)g''-g'^2-Mg'=0 \quad (15)$$

$$(1+\varepsilon_1\theta)\theta''+Rd\theta''+Pr(Nb(1+\varepsilon_2\phi)\phi'\theta'+(Nt+\varepsilon_1)\theta'^2+(f+g)\theta')+M\left(Ec_x f'^2+Ec_y g'^2\right)=0 \quad (16)$$

$$\phi''(1+\varepsilon_2\phi)+\varepsilon_2\phi'^2+Sc\left((f+g)\phi'-K_r\phi\right)+\frac{Nt}{Nb}\theta''=0 \quad (17)$$

Boundary conditions transformed as:

$$\left.\begin{array}{c} f=g=0, f'(0)=K_1 f''(0)+1, g'(0)=(K_2 g''+1)\delta,\ \theta'(0)=-Bi\left(1-\theta(0)\right), \\ Nb\phi'(0)+Nt\theta'(0)=0, f(\infty)\to 0, g(\infty)\to 0, \theta(\infty)\to 0, \phi(\infty)\to 0 \end{array}\right\} \quad (18)$$

For slip parameters, use K_1 and K_2, We Wiesenberger number Schmidt number is denoted Sc, Thermophoresis factor Nt, Thermal radiation factor Rd, Ec_x Eckert number in x axis, Ec_y Eckert number in y axis, the Prandtl number is Pr, The fluid viscosity is represented by θ_r, Brownian diffusion factor is Nb, chemical process K_r, Magnetic field parameter M, Biot number Bi, δ is stretching rate / ratio parameter,

$\theta_r=\frac{T_r-T_\infty}{T_w-T_\infty},\ Pr=\frac{\nu_f}{\alpha_f}, K_1=k_1\sqrt{\frac{a}{\nu_f}}, K_2=\frac{k_2 a}{\delta}\left(\sqrt{\frac{a}{\nu_f}}\right), Bi=\frac{h_f}{k_f}\sqrt{\frac{\nu_f}{a}}, \delta=\frac{b}{a}, M=\frac{\sigma B_0^2}{\rho_f a}, Sc=\frac{\nu_f}{D_{Bf}}, Nb=\frac{\tau D_B(C_w-C_\infty)}{\nu_f}, Nt=\frac{\tau D_T(T_w-T_\infty)}{T_\infty \nu_f}, We=\sqrt{\frac{2}{\nu_f}}ax\Gamma, Rd=\frac{16\sigma T_\infty^3}{3k^* k_f}.$

Physical quantities are the surface skin friction coefficient C_{fx}, C_{fy} and the local heat flux Nu_x are defined as

$$C_{fx}=\frac{\nu_f \tau_{wx}}{u_w^2}, C_{fy}=\frac{\nu_f \tau_{wy}}{v_w^2}\ Nu_x=\frac{xJ_w}{\alpha_f(T_w-T_\infty)}$$

$$\left.\begin{array}{c} \tau_{wx}=\mu_f\left(\frac{\partial u}{\partial z}+\frac{\Gamma}{\sqrt{2}}\left(\frac{\partial u}{\partial z}\right)^2\right)_{z=0} \\ \tau_{wy}=\mu_f\left(\frac{\partial v}{\partial z}+\frac{\Gamma}{\sqrt{2}}\left(\frac{\partial u}{\partial z}\right)^2\right)_{z=0} \\ J_w=-\alpha_f\left(\frac{\partial T}{\partial z}\right)_{z=0} \end{array}\right\} \quad (19)$$

Transformed quantities are

$$\left.\begin{array}{c} Re_x^{0.5}C_{fx}=\{f''(0)+Wef''(0)^2\} \\ Re_x^{0.5}C_{fy}=\{g''(0)+Weg''(0)^2\} \\ Re_x^{-0.5}Nu_x=-(1+Rd)\theta'(0) \\ Re_x^{-0.5}Sh_x=-\phi'(0) \end{array}\right\} \quad (20)$$

Re_x & Re_y Represents local Reynolds number

3. Numerical Algorithm

Higher-order differential equations are transformed into a set of first-order ODEs. Use the MATLAB bvp4c function to numerically solve the boundary value problem (BVP). Grid analysis verifies the

solution's dependability and precision. The bvp4c function effectively manages the modified first-order ODEs and boundary conditions.

4. Results and discussions

Figure 2 and 3 present the results of the inquiry into how the magnetic number and Williamson parameter affect velocity in the X and Y directions, respectively. Lorentz forces provide an inverse relationship between the magnetic number and the velocity in the X and Y directions. The velocity is slowed down in the X and Y axes directions by the Williamson parameter augmentation. Williamson parameter and viscosity are directly related. The fluid's velocity slows down as a result of its viscosity. The presence of the stretching ratio parameter delta on g', the slip constants K_1 on f', and K_2 on g', along with higher magnetic parameter values, result in a strong Lorentz force that drives liquid motion, as seen in Figure 4 and 5. As a consequence, decrease the velocity profiles for slips and increases with stretching ratio parameter. When the radiation and magnetic parameters are augmented and their impact on temperature is investigated in Figure 6, it is discovered that they are exactly proportional to one another. The Eckert number influence on the temperature profile is seen in Figure 7. The combination of thermal diffusion, cooling mechanisms, and viscous dissipation may cause the total temperature profile to show a slower rate of decline, even though a higher Eckert number typically indicates a faster conversion of kinetic energy to thermal energy.

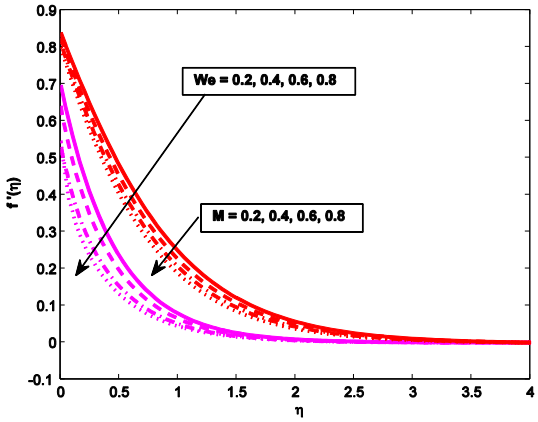

Figure.2 impact of We, M on $f'(\eta)$

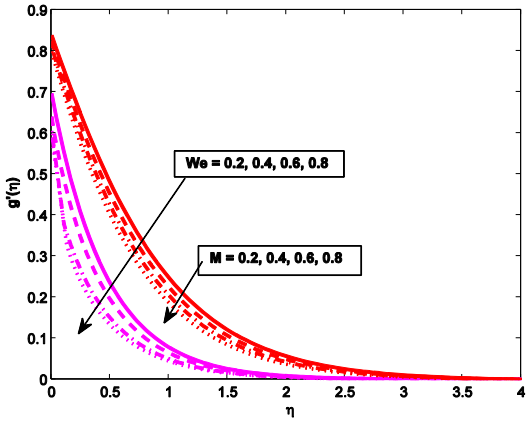

Figure.3 Impact of We, M on $g'(\eta)$

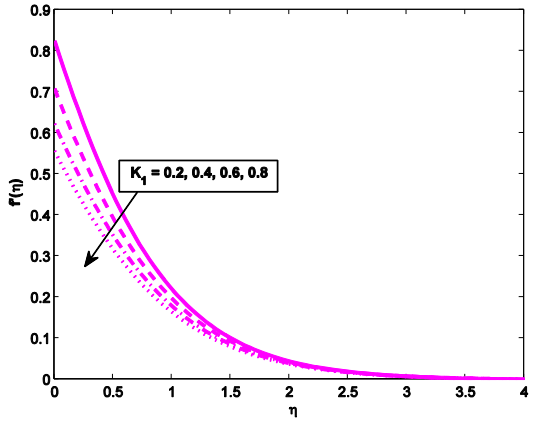

Figure.4 Impact of K_1 on $f'(\eta)$

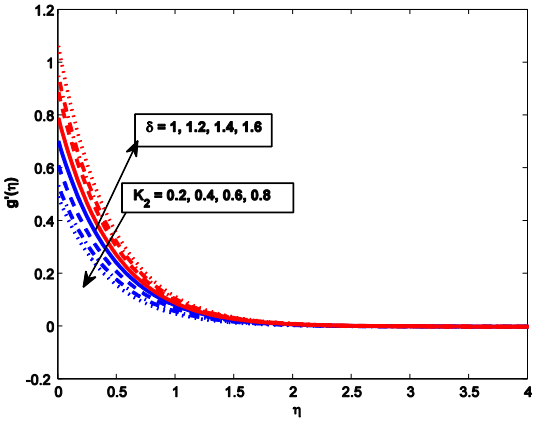

Figure.5 Impact of K_2, δ on $g'(\eta)$

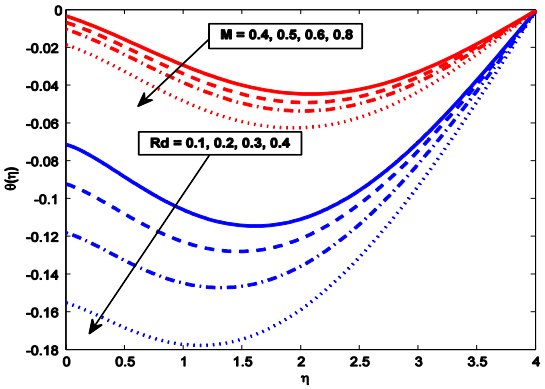

Figure.6 Impact of M, Rd on $\theta(\eta)$

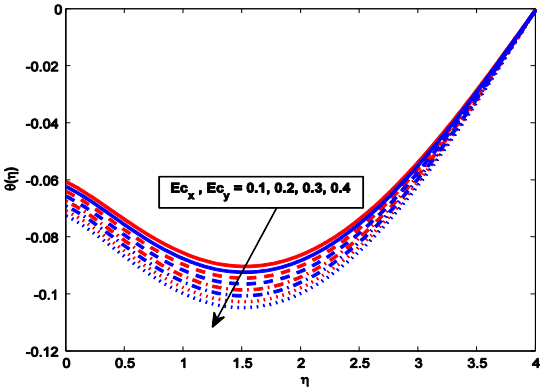

Figure.7 Impact of Ecx, Ecy on $\theta(\eta)$

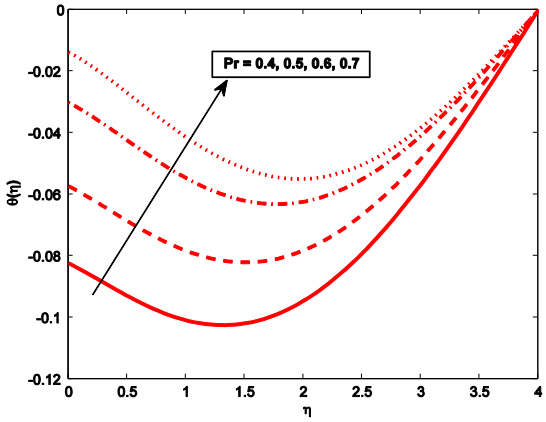

Figure.8 Impact of Pr on $\theta(\eta)$

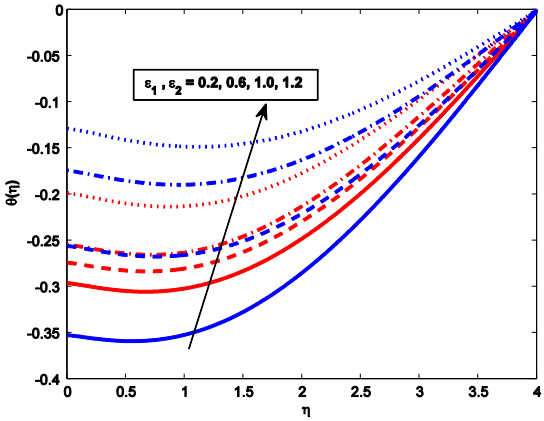

Figure.9 Impact of $\varepsilon_1, \varepsilon_2$ on $\theta(\eta)$

Figure 8 shows variations in Pr on the temperature distribution. The profile theta is shown to shrink with increasing Pr values. Pr values physically signify a strong momentum diffusivity that enhances the fluid temperature. Therefore, the thermal diffusivity and the thermal boundary layer thickness of Pr are inverse proportional. The impact on variable species diffusivity parameter ε_2 and variable thermal conductivity parameter $\varepsilon_1$on the temperature profile is shown in Figure 9. With an improvement, the temperature profile ε_1 and ε_2 values rose.

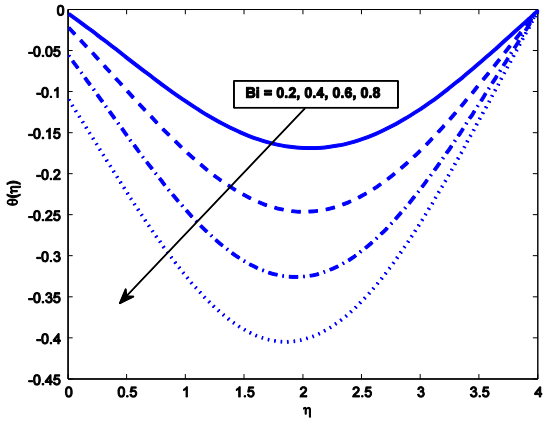

Figure.10 Impact of Bi on $\theta(\eta)$

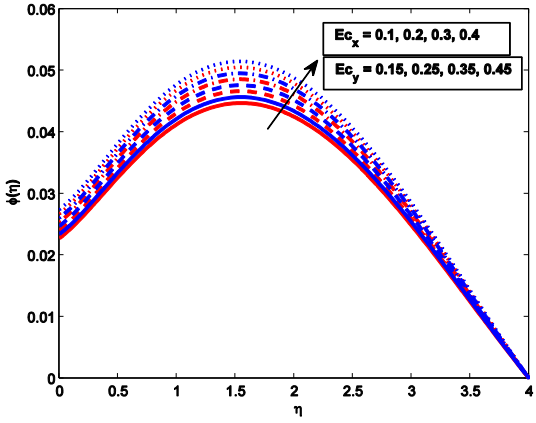

Figure.11 Impact of Ecx, Ecy on $\phi(\eta)$

Figure 10 illustrates how Biot number Bi affects the temperature profile. While increasing Bi thickens the thermal boundary layer and causes a fall in the temperature profile, raising Bi results in a decrease in the temperature profile. The reason for this is that bi is inversely proportional to thermal conductivity. The concentration profile is enhanced by Ec_x and Ec_y increase, as illustrated in Figure 11.

Figure 12 depicts how varied species diffusivity factor $\varepsilon_2$and variable thermal conductivity factor ε_1 affect the concentration profile. As the concentration profile diminished the $\varepsilon_1$and $\varepsilon_2$values increased. Figure 13 illustrates the effect of Kr (chemical reaction) and Sc (Schmidt number) on $\phi(\eta)$. Increasing Kr and Sc reduces nanoparticle concentration. Sc is defined physically as the ratio of viscous and molecular diffusion rates. Increasing the Schmidt number reduces mass diffusivity, which causes the concentration sketch for Sc to decrease.

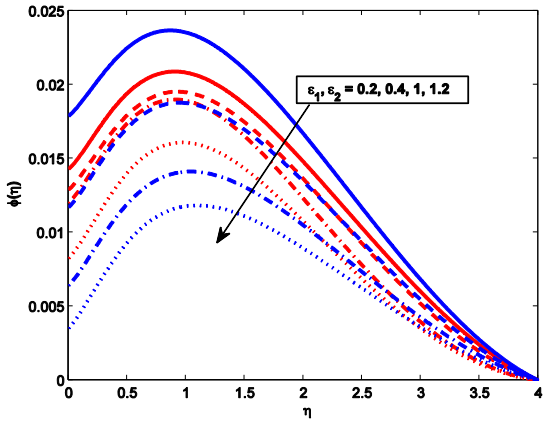

Figure.12 Impact of $\varepsilon_1, \varepsilon_2$ on $\phi(\eta)$

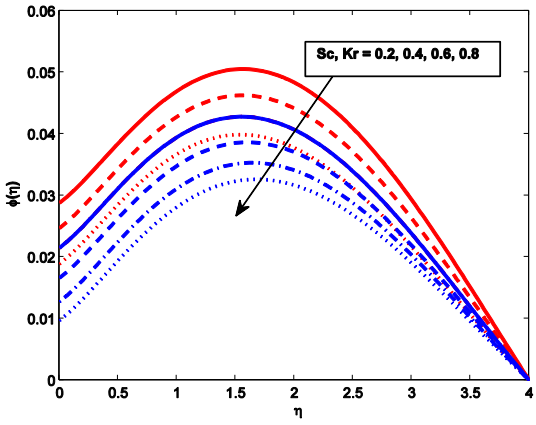

Figure.13 Impact of Sc, Kr on $\phi(\eta)$

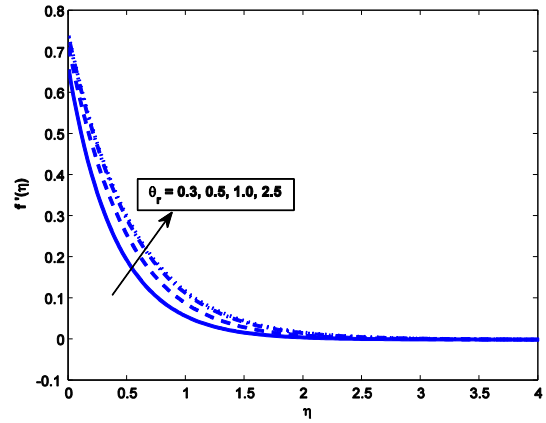

Figure.14 Impact of viscosity parameter on $f'(\eta)$ on $g'(\eta)$.

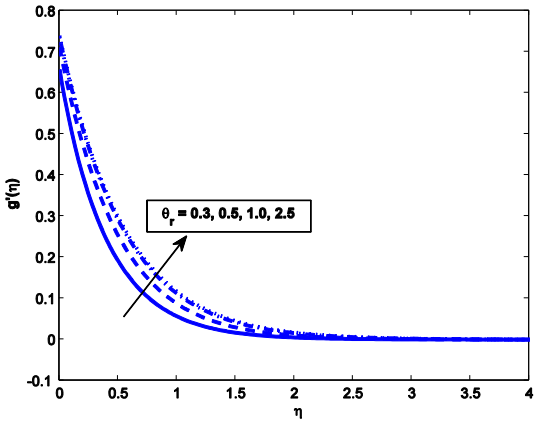

Figure.15 Impact of variable viscosity parameter

Figure 14 &15 illustrate the impact of viscosity parameter θ_r on fluid velocities $f'(\eta)$ and $g'(\eta)$ respectively, increasing values of θ_r enhances the fluid motion on x, y- directional velocities. Momentum Boundary layer thickness decreases while increasing viscosity parameter increases.

Table 1. Comparison of skin friction coefficient for $We = K_1 = K_2 = M = 0,\ \theta_r = 0$ for different values of velocity ratio parameter.

δ	Wang [24]		Present results	
	$-f''(0)$	$-g''(0)$	$-f''(0)$	$-g''(0)$
0.0	1.000000	0.000000	1.000000	0.000000
0.2	1.039511	1.148745	1.039143	1.147738
0.4	1.075765	1.349214	1.075016	1.340786
0.6	1.109951	1.560532	1.109932	1.596173
0.8	1.142491	0.866685	1.142482	0.860629
1.0	1.173722	1.173722	1.173742	1.083780

Table 2. Computing values of $Re_x^{-0.5}Sh_x$ in relation to various estimates of Sc, Kr, $\varepsilon_1, \varepsilon_2$, Nt.

Sc	Kr	ε_2	ε_1	Nt	$Re_x^{-0.5}Sh_x$
0.4	0.2	0.3	0.2	0.2	0.931725
0.5					0.803549
0.6					0.571101
	0.5				0.543284
	0.8				0.618974
		0.4			0.609807
		0.5			0.649579

Table 3. Computing values of $Re_x^{-0.5}Nu_x$ in relation to various estimates of Nt, Nb, Rd, Pr, Bi, $\varepsilon_1, \varepsilon_2$, M, Ec_x, Ec_y

Pr	Bi	Rd	Nt	Nb	M	ε_1	ε_2	Ec_x	Ec_y	$Re_x^{-0.5}Nu_x$
3	0.2	0.3	0.2	0.4	2	0.3	0.3	1	1	0.427824
4										0.430930
4.5										0.476731
	0.3									0.489788
	0.4									0.661929
	0.5									0.893992
		0.3								0.417120
		0.4								0.490633
		0.5								0.725826
			0.3							0.573341
			0.4							0.568533
				0.4						0.571806
				0.6						0.557728
					3					0.473318
					4					0.491645
					5					1.587171
						0.4				0.544124

						0.5				0.584008
						0.6				0.636663
							0.4			0.591191
							0.5			0.568432
							0.6			0.525145

5. Conclusion

This paper examines the numerical analysis of a 3D MHD Williamson nanofluid flowing over a stretched sheet with varying thermal conductivity and diffusivity under thermal radiation, velocity slip, and convective boundary conditions. We suggested a modified RK-4th order numerical approach, bvp4c shooting technique, to solve the problem using the created mathematical model. The most significant points are noted below.

i. The x and y velocities drop down progressively due to magnetic field effects and the Williamson fluid parameter.
ii. The behavior of the temperature field dims as the values of M, Rd, Ec increase, however the reverse behavior is found with higher values of Pr, Bi, variable thermal conductivity, and variable species diffusivity.
iii. Higher viscosity suggests higher internal friction throughout the fluid, slowing the flow of fluid particles and reducing velocity.
iv. Concentration distribution is lowered by the first-order chemical reaction's increasing rate and Schmidt number Sc.

References

[1] Maria, Imtiaz. (2023). Impact of magnetohydrodynamics in bidirectional slip flow of Maxwell fluid subject to stretching, radiation, and variable properties. Numerical Heat Transfer Part A-applications, doi: 10.1080/10407782.2023.2176383

[2] Upreti, H., Bisht, A., & Joshi, N. (2024). MHD Darcy–Forchheimer flow and double-diffusive modeling of Maxwell fluid over rotating stretchable surface: A computational study. Modern Physics Letters B. https://doi.org/10.1142/s0217984924502270

[3] Sinha, A., Misra, J., & Shit, G. (2016). Effect of heat transfer on unsteady MHD flow of blood in a permeable vessel in the presence of non-uniform heat source. Alexandria Engineering Journal, 55(3), 2023–2033. https://doi.org/10.1016/j.aej.2016.07.010

[4] Murtaza, M. G., Jahangircu, Ferdows, M., Tzirtzilakis, E. E., & Shamshuddin, M. (2023). (0040) Effects of Variable Fluid Properties and Mixed Convection on Biomagnetic Fluid Flow and Heat Transfer over a Stretching Sheet in the presence of Magnetic Dipole. Authorea (Authorea). https://doi.org/10.22541/essoar.170264373.31639349/v1

[5] Muzemder, A. S. H., & Singh, K. (2024). Influence of sedimentary structure and pore-size distribution on upscaling permeability and flow enhancement due to liquid boundary slip: A pore-scale computational study. Advances in Water Resources, 190, 104752. https://doi.org/10.1016/j.advwatres.2024.104752

[6] Fara, J., Hron, J., Málek, J., Rajagopal, K., & Tůma, K. (2024). Fluid–structure numerical solver for axi-symmetric flows with Navier's slip interface condition between the viscoelastic solid and the Navier–Stokes fluid: Effects of deformable solids on the flow characteristics. International Journal of Engineering Science, 201, 104088. https://doi.org/10.1016/j.ijengsci.2024.104088

[7] Sudarmozhi, K., Iranian, D., & Khan, I. (2023). A steady flow of MHD Maxwell viscoelastic fluid on a flat porous plate with the outcome of radiation and heat generation. Frontiers in Physics, 11. https://doi.org/10.3389/fphy.2023.1126662

[8] Muhammad, N., Almutairi, S., Sarfraz, M., Saleem, S., & Khan, M. (2024). Exploring cubic kinetics in viscoelastic fluid flow with thermal viscous dissipation on a stretching surface. Chemical Physics Letters, 849, 141420. https://doi.org/10.1016/j.cplett.2024.141420

[9] Choudhari, R., Vaidya, H., Prasad, K. V., Gulab, R. K., Guedri, K., Rehman, A., & Galal, A. M. (2022). Electroosmosis Augmented MHD Third-Grade Fluid with Slip and Variable Properties: An Application for Blood Flow in Arteries. Journal of Computational Biophysics and Chemistry, 22(03), 243–258. https://doi.org/10.1142/s273741652340001x

[10] Taneja, S., Poply, V., & Kumar, P. (2022). Fluid properties of an unsteady MHD free stream flow over a stretching sheet in presence of radiation. Heat Transfer, 52(3), 2383–2399. https://doi.org/10.1002/htj.22788

[11] Tarakaramu, N., Narayana, P. S., & Venkateswarlu, B. (2020). Numerical simulation of variable thermal conductivity on 3D flow of nanofluid over a stretching sheet. Nonlinear Engineering, 9(1), 233–243. https://doi.org/10.1515/nleng-2020-0011

[12] C, S. R., Naikoti, K., & Rashidi, M. M. (2017). MHD flow and heat transfer characteristics of Williamson nanofluid over a stretching sheet with variable thickness and variable thermal conductivity. Transactions of a Razmadze Mathematical Institute, 171(2), 195–211. https://doi.org/10.1016/j.trmi.2017.02.004

[13] Sun, B., Peng, C., Zuo, R., Yang, D., & Li, H. (2016). Investigation on the flow and convective heat transfer characteristics of nanofluids in the plate heat exchanger. Experimental Thermal and Fluid Science, 76, 75–86. https://doi.org/10.1016/j.expthermflusci.2016.03.005

[14] Sheikholeslami, M., & Rokni, H. B. (2017). Effect of melting heat transfer on nanofluid flow in existence of magnetic field considering Buongiorno Model. Chinese Journal of Physics, 55(4), 1115–1126. https://doi.org/10.1016/j.cjph.2017.04.019

[15] Prasannakumara, B. C., Ramesh, K., Kumar, R. N., & Gowda, R. J. P. (2023). 3D Boundary Layer Flow of Conducting Nanoliquid Over a Stretching Sheet with Homogeneous and Heterogeneous Reactions. In CRC Press eBooks (pp. 363–380). https://doi.org/10.1201/9781003299608-21

[16] Alhazmi, M., & Ahmed, S. E. (2024). 3D flow of variable properties viscoelastic nanofluids with impacts of Arrhenius energy and Cattaneo–Christov double-diffusion. Numerical Heat Transfer Part a Applications, 1–20. https://doi.org/10.1080/10407782.2024.2310602

[17] Rafique, K., Mahmood, Z., & Khan, U. (2023). Mathematical analysis of MHD hybrid nanofluid flow with variable viscosity and slip conditions over a stretching surface. Materials Today Communications, 36, 106692. https://doi.org/10.1016/j.mtcomm.2023.106692

[18] Aziz, A., Hussain, S. T., & Sadiq, A. (2023). Mathematical model for a thermal cooling system with variable viscosity and thermal conductivity over a rotating disk. Case Studies in Thermal Engineering, 52, 103664. https://doi.org/10.1016/j.csite.2023.103664

[19] Mishra, N. K., Sharma, M., Sharma, B. K., & Khanduri, U. (2023). Soret and Dufour effects on MHD nanofluid flow of blood through a stenosed artery with variable viscosity. International Journal of Modern Physics B, 37(30). https://doi.org/10.1142/s0217979223502661

[20] Rehman, A., Khun, M. C., Alotaibi, H., & Inc, M. (2024). The influence of Marangoni convection in engine oil base nanofluid with the impact of variable viscosity and viscous dissipation on infinite disk. ZAMM - Journal of Applied Mathematics and Mechanics / Zeitschrift Für Angewandte Mathematik Und Mechanik. https://doi.org/10.1002/zamm.202300556

[21] Ali, L., Liu, X., & Ali, B. (2020). Finite Element Analysis of Variable Viscosity Impact on MHD Flow and Heat Transfer of Nanofluid Using the Cattaneo–Christov Model. Coatings, 10(4), 395. https://doi.org/10.3390/coatings10040395

[22] Basha, H. (2024). Significance of Variability in Liquid Properties on 3D MHD Maxwell Nanofluid Flows Over a Stretching Surface with Heat Generation/Absorption and Chemical Reaction. Journal of Nanofluids, 13(1), 15–27. https://doi.org/10.1166/jon.2024.2124

[23] Vaidya, H., Prasad, K. V., Vajravelu, K., Shehzad, S. A., & Basha, H. (2018). Role of Variable Liquid Properties in 3D Flow of Maxwell Nanofluid Over Convectively Heated Surface: Optimal Solutions. Journal of Nanofluids, 8(5), 1133–1146. https://doi.org/10.1166/jon.2019.1658

[24] Wang, C. Y. (1984). The three-dimensional flow due to a stretching flat surface. The Physics of Fluids, 27(8), 1915–1917. https://doi.org/10.1063/1.864868